

Bragg scattering from a weak random potential

Donghwan Kim

*Department of Chemistry and Chemical Biology,
Harvard University, Cambridge, Massachusetts 02138, USA*

Eric J. Heller*

*Department of Physics, Harvard University, Cambridge, Massachusetts 02138, USA and
Department of Chemistry and Chemical Biology,
Harvard University, Cambridge, Massachusetts 02138, USA*

(Dated: September 20, 2021)

A potential for a propagation of a wave in 2D is constructed from a random superposition of plane waves around all propagation angles. Surprisingly, sharp diffraction of the wave is observed, analogous to crystal or powder diffraction pattern. The scattering is partially resonant, so Fermi's golden rule does not apply.

It is well-known that monochromatic light or matter waves entering a perfectly periodic medium show sharp Bragg scattering into specific angles. Randomly disturbing the perfect lattice positions leads to diffuse scattering between the Bragg peaks. As the dispersion increases the diffuse scattering eventually dominates, and finally the Bragg peaks vanish. The diffuse scattering is structured, revealing correlations in the medium. For example, for X-ray scattering in water, the pair correlation function has a broad peak with a characteristic length scale, which in turn generates a broad peak in the structure function [1, 2].

It is not expected however that a random medium, with no perfect order on any scale, can generate sharp scattering angles, yet we report such a case here. For the potential we choose, the spatial autocorrelation function has broad peaks as in water, but the scattering cross section nonetheless has very sharp peaks, with scattering only at certain angles relative to the incident beam. This is startling; the scattering in the random potential defined below is like Bragg scattering in a periodic potential, rather than the scattering in a correlated liquid. The closest analog, though not a perfect one, is powder diffraction, with many randomly oriented crystallites packed closely. The potential we define below has no such "crystallites," yet it has Bragg peaks.

This surprise can be explained by calculation of scattering matrix elements, or equivalently by examining the Fourier components of the potential.

The time evolution of the scattering discussed below does not however obey Fermi's golden rule, so the matrix elements are not the whole story. Given an incident wavepacket of well defined momentum, the population growth of the Bragg-like scattered wave is oscillatory, like a resonant double well. The Bragg-like scattering develops quickly, as befits a resonant process. Starting with a wavepacket having a well defined direction of propagation, sporadic "Bragg pulses" emerge from it (see e.g. FIG. 3 and 5).

We consider a random potential with the following

form.

$$V(\vec{r}; \{\phi_j\}) = \frac{A}{\sqrt{N}} \sum_{j=1}^N \cos(\vec{q}_j \cdot \vec{r} + \phi_j) \quad (1)$$

where A is a constant having the dimension of energy, N is the number of modes, $\vec{q}_j = q(\hat{x} \cos \theta_j + \hat{y} \sin \theta_j)$, and $\theta_j = 2\pi(j-1)/N$. This is a superposition of N plane waves of an equal amplitude A and wavenumber q each propagates in different directions with an angle θ_j and a random phase shift ϕ_j . We call it a "Berry potential," a function introduced in connection with wave chaos [3, 4]. The normalization factor $1/\sqrt{N}$ is introduced, making the average fluctuation $V_{rms} = \sqrt{\langle (V(\vec{r}; \{\phi_j\}))^2 \rangle}$ independent of the number of modes N .

The spatial autocorrelation of the potential function is

$$C(\delta\vec{r}) = \langle V(\vec{r})V(\vec{r} + \delta\vec{r}) \rangle = \frac{A^2}{N} \sum_{j=1}^N \cos(\vec{q}_j \cdot \delta\vec{r})/2$$

In the limit of many modes $N \gg 1$ and for $\Delta\theta = 2\pi/N$,

$$C(\delta\vec{r}) \approx \frac{A^2}{2\pi} \int_0^{2\pi} d\theta \cos(q\delta r \cos \theta)/2 = \frac{A^2}{2} J_0(q\delta r)$$

where J_0 is the Bessel function of the first kind of order 0. The autocorrelation function of the Berry potential is shown in FIG. 1. Note the peaks give characteristic length scales shown in the potential plot in FIG. 2.

Now we propagate wave packets of fairly well defined momentum $\hbar\vec{k}$ in the potential $V(\vec{r})$. We use a second order split operator method [6] where the time evolution operator for the Hamiltonian $H = T + V$ where T and V are kinetic and potential energy operators, respectively, is approximated as

$$e^{-iH\Delta t/\hbar} = e^{-iV\Delta t/2\hbar} e^{-iT\Delta t/\hbar} e^{-iV\Delta t/2\hbar} + \mathcal{O}((\Delta t)^3)$$

Consider launching a wave of an initial average wavenumber k into the Berry potential. To have a

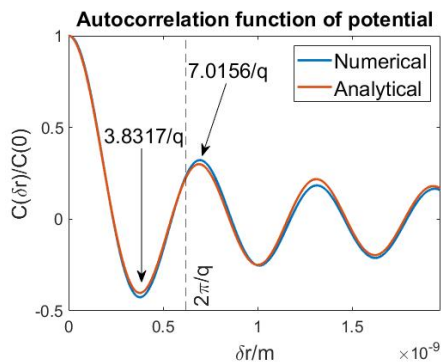


FIG. 1. The (normalized) spatial autocorrelation function of the Berry potential. Numerical result and the evaluation of the analytical expression $J_0(q\delta r)$ match well. Two peaks at $\delta r = 3.8317/q, 7.0156/q$ give characteristic length scales in the potential plot in real space shown in FIG. 2. Note the first positive peak at $\delta r = 7.0156/q$ is slightly off from the wavelength $2\pi/q$ of each sinusoid of the potential, shown as a vertical dashed line.

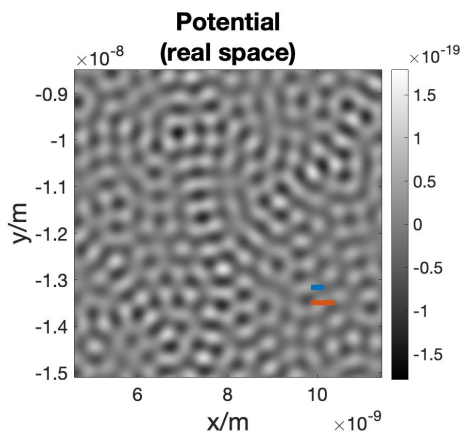


FIG. 2. Plot of the Berry potential in real space. Thick blue and red lines show the characteristic lengths from the two peaks at $\delta r = 3.8317/q$ and $7.0156/q$, respectively, of the autocorrelation function shown in FIG. 1. The distance between a white bump and an adjacent black dip indeed matches with the length of the blue line. Also, the distance between adjacent white bumps (or black dips) agrees with the length of the red line.

“weak” potential, set the constant A such that the fluctuation of the potential V_{rms} to be far smaller than the average kinetic energy of the wave $E_{kin} = \frac{\hbar^2 k^2}{2m}$, i.e., $V_{rms} \ll E_{kin}$. The scattering behavior of the wave varies considerably depending on the wavelength of the wave $2\pi/k$ compared to the wavelength of the sinusoids $2\pi/q$ used in the Berry potential.

Figure 3 shows the Berry potential in grayscale. The inset shows the probability distribution of the wave in the reciprocal space. The top panel depicts an initial wavepacket launched downward into the potential with an average momentum. As time goes by, as shown in, as shown in

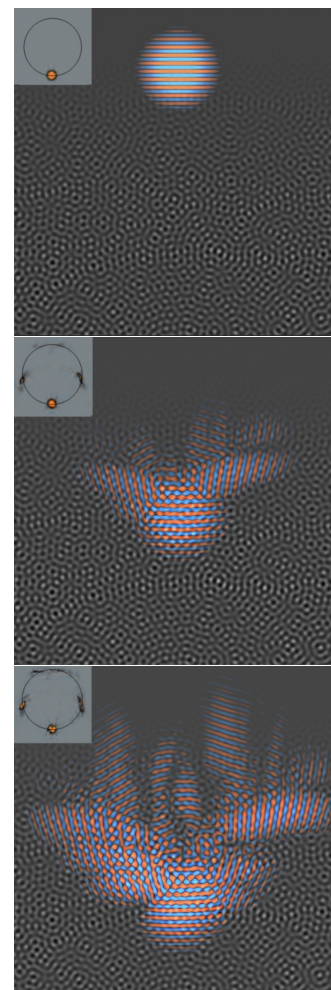


FIG. 3. Bragg scattering in a random (Berry) potential. The potential was drawn in grayscale and the real part of the wavefunction was plotted in red/blue scale. The inset shows the probability distribution of the wave in the reciprocal space. The top panel depicts an initial wavepacket launched downward into the potential with an average momentum. As time goes by, as shown in the middle panel, the wave is scattered by the random potential, but only to the Bragg angle. One can also clearly see this in the reciprocal space where the scattered waves are populated at Bragg angle. Later, as shown on the bottom panel, the scattered wave scatters again with the same Bragg angle.

the middle panel, the wave is scattered by the random potential, but only to the Bragg angle. One can also clearly see this in the reciprocal space where the scattered waves are populated at Bragg angle. Later, as shown on the bottom panel, the scattered wave scatters again with the same Bragg angle. This is a multiple scattering, not a higher order Bragg scattering which is absent if the Berry potential is composed only of sinusoids. The higher order scattering would be allowed if instead triangular waves were used, for example.

The Bragg scattering of the wave in Berry poten-

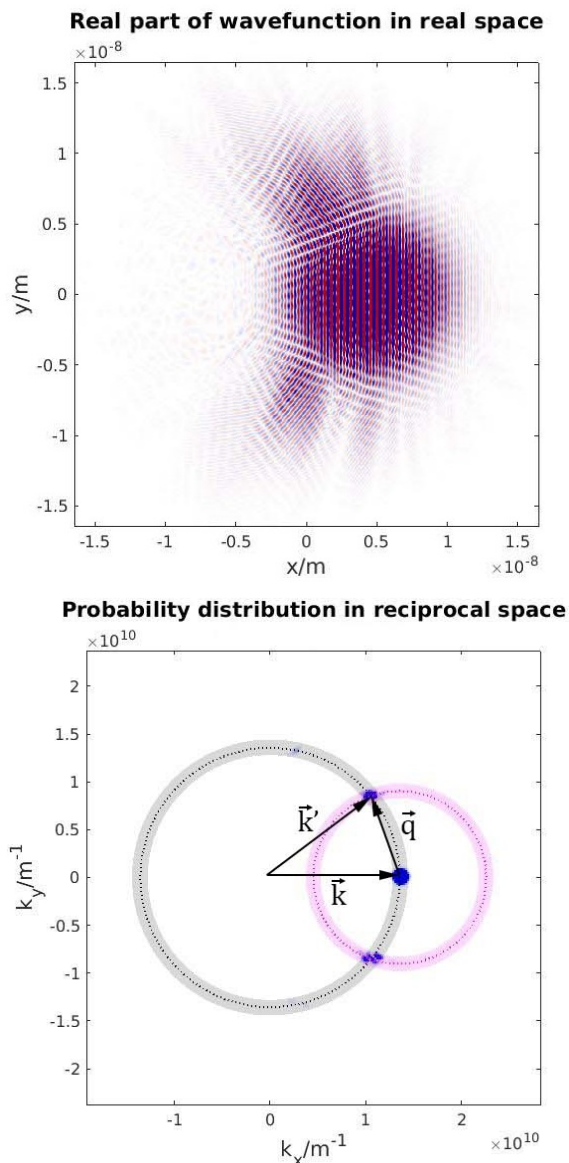


FIG. 4. Real (top) and reciprocal (bottom) space pictures of the wave. The top panel shows the real part of the wavefunction, where the colormap range is chosen to show the “Bragg wings” better. The bottom panel shows the probability density distribution in the reciprocal space with blue scale. The initial \vec{k} , final \vec{k}' , scattering \vec{q} wavevectors are shown. For a given initial wavevector \vec{k} , the contour of equal energy can be drawn as a black dotted line. In addition, taking \vec{k} as an origin, the nonzero Fourier components of the potential can be drawn as a magenta dotted line. The Bragg scattered states appear at the intersecting points of the black and magenta dotted lines. As the initial wavefunction has the momentum spread, \vec{k} can be chosen to be any wavevector near the average value $\langle \vec{k} \rangle$. The shaded gray and magenta area are the area covered by the collection of the black and magenta dotted lines, respectively, considering all of the initial wavevector \vec{k} near the average value $\langle \vec{k} \rangle$.

tial can roughly be thought as a superposition of the scattered waves by each constituent sinusoidal potential aligned in different directions. The situation is analogous to the powder X-ray diffraction in which crystallites are aligned in all possible orientations, leading to the incoherent superposition of the outgoing waves from scattering by the crystallites. The standard picture is the scattering by some of the crystallites oriented properly with respect to incident X-ray beam leads to Bragg scattering, although this view has been challenged [7] in ways that are relevant to our present observations. Again there are no crystallites here, but the Berry potential bears some relation to the impossible limit of overlapping and blending them.

Using this analogy, by treating the wavelength $2\pi/q$ of the single sinusoid in the Berry potential as a “lattice spacing”, one can write down Bragg condition $n(2\pi/k) = 2(2\pi/q) \sin \theta$, which correctly explains our simulation result. Numerically, only $n = 1$ Bragg angle was observed. Higher order $n = 2, 3, \dots$ Bragg angles will be observed if triangular, instead of sinusoidal, waves are used. Let’s denote $n = 1$ Bragg angle as $\theta_B = \sin^{-1}(q/2k)$. $n = 1$ Bragg scattering occurs several times as can be seen from the bottom panel of Figure 3. However, this analogy is not perfect since, in the random Berry potential, the superposition of the scattered waves by each sinusoidal component is coherent, rather than incoherent which was the case in the powder diffraction as the phases of scattered waves from one crystallite to another do not match. The Berry potential coherence effect is manifested in the population growth of the scattered wave, as explained in the section below.

The spatial autocorrelation function of the Berry potential is a Bessel function $C(\delta\vec{r}) \propto J_0(q\delta r)$. Since it has a positive broad peak at $q\delta r = 7.0156$ (as shown in FIG. 1), one may regard δr near $7.0156/q$ as a “lattice spacing” and predict a broad peak in the scattering cross section near Bragg angle θ satisfying the Bragg condition $(2\pi/k) = 2(7.0156/q) \sin \theta$. However, this does not explain the actual angular distribution of the wave. The autocorrelation function fails to explain both the peak position and the width of the scattering correctly. Instead very sharp peaks at Bragg angles θ satisfying $(2\pi/k) = 2(2\pi/q) \sin \theta$ are seen. The random Berry “medium” has no special directions of travel; all are equivalent and subject to Bragg diffraction at *relative* angle θ . This means correct “lattice spacing” is the wavelength $2\pi/q$ of the single sinusoid, not the first positive peak of the autocorrelation at $7.0156/q$. This indicates we need to look at other quantities rather than the autocorrelation.

Consider scattering matrix element $\langle \vec{k}' | V | \vec{k} \rangle \sim V_{\vec{k}' - \vec{k}}$ where $|\vec{k}\rangle$ is a plane wave state and $V_{\vec{k}' - \vec{k}}$ is the Fourier component of the potential. It needs a nonzero Fourier component, $V_{\vec{k}' - \vec{k}} \neq 0$ for the scattering to happen. As-

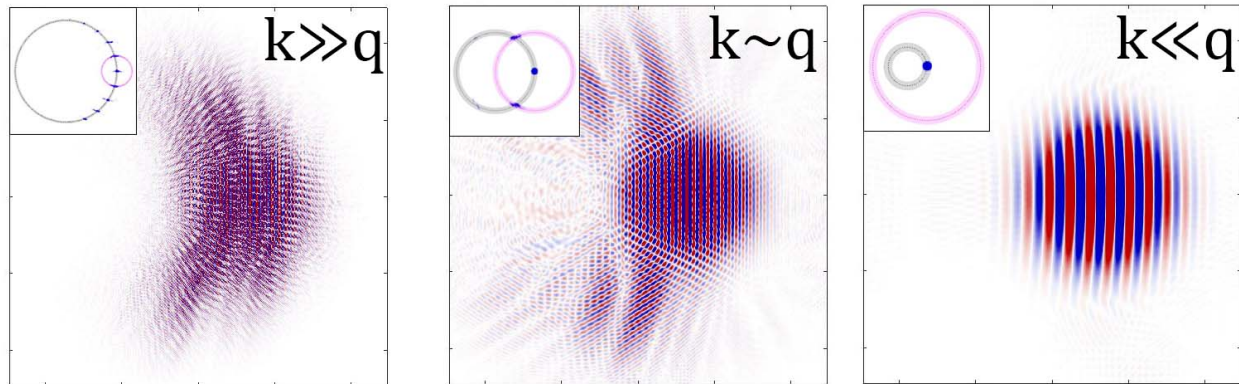


FIG. 5. Various physical regimes depending on the \hbar value. The real part of the wavefunction was plotted in red/blue scale and a small inset on the upper left of each panel shows the probability density distribution in the reciprocal space. For small \hbar , *i.e.*, $k \gg q$ (small wavelength and classical limit), the wave is particle-like, diffusive, showing branched flow [5]. This is explained by the small Bragg angle which leads to almost-forward scattering. For intermediate \hbar , *i.e.*, $k \sim q$ the wave interference is significant and sharp Bragg scattering is observed. The Bragg angle is not small, so it shows a diffractive behavior, looking less classical. For large \hbar , *i.e.*, $k \ll q$ the wave is in transparency regime since the wavelength is so large that the fluctuations of the potential is effectively averaged out to zero. Or equivalently, in reciprocal space the intersecting points between the energy contour and the nonzero Fourier component of the potential are nonexistent, so there is no scattering and the potential is transparent.

suming elastic scattering, the scattering wavevector $\vec{q} = \vec{k}' - \vec{k}$ and scattering angle 2θ satisfy $q = 2k \sin \theta$, which is the same as the Bragg condition $n(2\pi/k) = 2(2\pi/q) \sin \theta$ for $n = 1$. This is why using the Bragg condition with the “lattice spacing” of the wavelength $2\pi/q$ of the sinusoid works. Thus, an allowed elastic scattering, which has a nonzero scattering matrix element, can actually be interpreted as a Bragg scattering by a “lattice” of the sinusoidal component, with a wavevector \vec{q} , of the potential.

Using the scattering matrix element analysis, one can draw nonzero Fourier components of the potential on the reciprocal space probability distribution plot as shown in FIG. 4. The simulation result shows the reciprocal space picture explains the scattering phenomenon correctly. The momentum dispersion of the initial wavepacket makes a small range of Bragg angles populated as explained in the caption of FIG. 4.

To see the effect of length scales, we compare wave scattering for different \hbar 's, keeping the average momentum of the wave $\hbar k$ fixed. Thus if \hbar increases by a factor of two, the wavenumber of the wave k decreases by a factor of two, and the wavelength increases by two, keeping the average momentum fixed.

Depending on the value of \hbar (so the wavelength), the wavepacket scattering exhibits qualitatively different behaviors as shown in FIG. 5. For small \hbar , *i.e.*, $k \gg q$ (small wavelength and classical limit), the wave is particle-like, diffusive, showing branched flow [5]. This is consistent with a very small Bragg angle which leads to almost-forward scattering. For intermediate \hbar , *i.e.*, $k \sim q$ the

Bragg angle is not small, so it shows diffractive behavior, looking less classical. For large \hbar , *i.e.*, $k \ll q$ the wave is in a transparency regime: the wavelength is large enough that the smaller scale fluctuations of the potential are averaged to zero. Or equivalently, in reciprocal space, there are no intersecting points between the energy contour and the Fourier component of the potential. There is no therefore scattering, and the potential is transparent.

One can calculate the population $\langle \psi^{(1)}(t) | \psi^{(1)}(t) \rangle$ of the scattered waves using 1st order time-dependent perturbation theory as the following [8]

$$\langle \psi^{(1)}(t) \rangle = \int_0^t \frac{dt'}{i\hbar} e^{-iT(t-t')/\hbar} V(t') e^{-iTt'/\hbar} |\psi(0)\rangle$$

In the Berry potential, the populations near the Bragg angle θ_B (so the scattering angle $2\theta_B$) were calculated in the simulation and compared with the perturbation theory as shown in FIG. 6.

One can clearly see the population growth is not linearly increasing, which means Fermi's golden rule is not working. This is because Fermi's golden rule assumes (1) the scattering to be from a single state to a continuum, and (2) the superposition of the scattered waves to be incoherent. Both are not true in this case; the scattering by the potential is from a single state to a single state, and the superposition of the scattered waves are coherent. The latter is why the population growth stops occasionally, or equivalently, the pulses (scattered waves) comes out sporadically.

This behavior is somewhere between Fermi's golden rule behavior and the double well potential behavior [8].

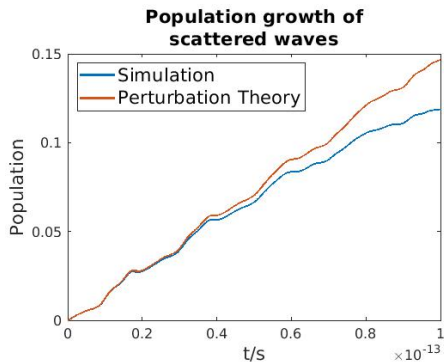


FIG. 6. Population of scattered waves as a function of time. Blue and red curves correspond to simulation and 1st order time-dependent perturbation theory results, respectively. One can clearly see the population growth is not linearly increasing, which means Fermi's golden rule is not working. Also, the population growth stops occasionally, showing that the pulses (scattered waves) comes out sporadically. The two results coincide at the early time as the single scattering dominates. The discrepancy later is due to multiple scattering in the simulation, which is absent in the 1st order time-dependent perturbation theory.

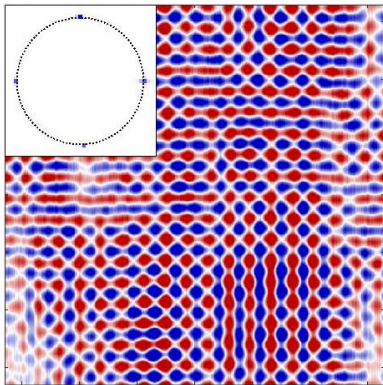


FIG. 7. Bragg scattering in a Berry potential: a special case of 90 degree scattering angle. The real part of the wavefunction was plotted in red/blue scale. The inset shows momentum space probability distribution of the wave. This is a snapshot, after long time propagation of a horizontally launched wavepacket. It is not diffusing in angle beyond the 90 degree turns, in spite of the random nature of the potential. A periodic boundary condition is used.

The double well potential has an oscillatory behavior due to the coherence. In addition, this effect arises since the potential in Eq. (1) fills a one dimensional curve in the Fourier space plane. If it starts filling areas, the effect will go away at some rate. Also, the population growth and scattering behavior depend largely on the size, shape and speed of the initial wave.

In addition, for special Bragg angles, there exists a momentum localization as shown in Fig. 7. A snapshot

of the wave is shown after long propagation of an initial wavepacket launched rightward, in a 90 degree scattering (45 degree Bragg angle) situation. Of course, the scattered wings again re-scatter at 90 degrees, and so on. There is possibly permanent localization only to vertical and horizontal motion.

If the diffraction angle is $2\pi/N$ where N is an integer, the scattered wave comes back to the original incident angle after N scatterings, thus the momentum distribution does not fill in the whole range of 2π . The special angles show localization of the wave in momentum space, assuming the initial wavepacket is narrow enough in momentum space.

The forementioned Bragg scattering from a weak random potential is experimentally realizable in a laser cavity with a single mode laser (need not be single) with rough or ballistically chaotic walls, so that the wave inside is a random superposition of waves traveling in all directions. Sending an atomic beam into the chaotic cavity would show scattering at Bragg angles.

The authors thank David Guéry-Odelin, Alvar Daza, Frans A. Spaepen, Paul F. Fewster and Joon-Suh Park for discussion and suggestion. We thank the NSF the Center for Integrated Quantum Materials (CIQM) Grant No. DMR-1231319.

* eheller@fas.harvard.edu

- [1] A. H. Narten, M. D. Danford, and H. A. Levy, X-ray diffraction study of liquid water in the temperature range 4–200°C, *Discuss. Faraday Soc.* **43**, 97 (1967).
- [2] A. H. Narten and H. A. Levy, Liquid water: Molecular correlation functions from x-ray diffraction, *The Journal of Chemical Physics* **55**, 2263 (1971), <https://doi.org/10.1063/1.1676403>.
- [3] M. V. Berry, Regular and irregular semiclassical wavefunctions, *Journal of Physics A: Mathematical and General* **10**, 2083 (1977).
- [4] M. S. Longuet-Higgins, *The Statistical Analysis of a Random, Moving Surface*, *Philosophical Transactions of the Royal Society of London. Series A, Mathematical and Physical Sciences* **249**, 321 (1957), publisher: The Royal Society.
- [5] M. A. Topinka, B. J. LeRoy, R. M. Westervelt, S. E. Shaw, R. Fleischmann, E. J. Heller, K. D. Maranowski, and A. C. Gossard, Coherent branched flow in a two-dimensional electron gas, *Nature* **410**, 183–186 (2001).
- [6] A. D. Bandrauk and H. Shen, Higher order exponential split operator method for solving time-dependent Schrödinger equations, *Canadian Journal of Chemistry* **70**, 555 (1992), <https://doi.org/10.1139/v92-078>.
- [7] P. F. Fewster, A new theory for x-ray diffraction, *Acta Crystallographica Section A Foundations and Advances* **70**, 257–282 (2014).
- [8] E. Heller, *The Semiclassical Way to Dynamics and Spectroscopy* (Princeton University Press, Princeton, NJ, 2018).